Advanced Steel Construction – Vol. 19 No. 1 (2023) 70–76
DOI:10.18057/IJASC.2023.19.1.9
(**Special Issue:** *10th International Conference on Advances in Steel Structures, ICASS'2020, Chengdu, China*)

MECHANICAL PROPERTIES AND SIMULATION METHOD OF STRUCTURAL STEEL AFTER HIGH CYCLE FATIGUE DAMAGE

Qi Si [1], Yang Ding [1, 2], Liang Zong [1, 2, *] and Heng Liu [1]

[1] *School of Civil Engineering, Tianjin Univ., Tianjin 300072, China.*
[2] *Key Laboratory of Coast Civil Structure Safety, Ministry of Education, Tianjin Univ., Tianjin 300072, China*
** (Corresponding author: E-mail: zongliang@tju.edu.cn)*

ABSTRACT

The steel structure will be subjected to alternating loads during its service, so the fatigue damage will gradually accumulate. Although fatigue damage may not cause immediate failure of the steel structure, the mechanical properties of the steel structure will inevitably be weakened. In this paper, the changes in mechanical properties of Q355B and Q690D steels after fatigue damage were investigated by static tensile tests. Then, a numerical simulation method for structural steel after fatigue damage was proposed. Finally, the results obtained from the finite element model were compared with the experimental results to verify the accuracy of the proposed numerical simulation method.

ARTICLE HISTORY

Received: 20 July 2022
Revised: 22 August 2022
Accepted: 10 January 2023

KEYWORDS

Steel structure;
Mechanical properties;
Simulation method;
Fatigue damage;
High cycle fatigue

1. Introduction

With the continuous development of Chinese infrastructure construction, steel structures are widely adopted in large-span space structures, bridge structures, marine engineering structures, and many other important projects with the advantages of lightweight, excellent mechanical properties, and recyclability. Steel structure engineering in its service period will be subject to long-term alternating loads such as vehicles, wind, waves, etc., which accumulate to form significant fatigue damage. Although fatigue damage may not cause immediate failure of the steel structure, the mechanical properties of the steel structure will inevitably be weakened under the effect of long-term cumulative damage, increasing the potential safety risks.

In recent years, the influence of fatigue damage on the mechanical properties of metal materials has attracted the attention of scholars at home and abroad, and related research has been carried out. In terms of experimental research, Moćko [1] studied the effects of pre-fatigue on the DP 500 steel during tensile tests at low and high strain rates. Cockings [2] studied the effect of pre-strain and pre-fatigue on the monotonic behavior of AerMet100, 300M, and MLX-17 steels. Zhang [3] studied the residual strength of Q690 high-strength steel with pre-fatigue damage through a static tensile test. Wu [4] studied the degradation mechanism of mechanical properties of 45 steel with different degrees of fatigue damage. Tang [5] investigated the influence of pre-fatigue damage on the mechanical properties of Q345 steel and studied the effects of the pre-damage levels on the ultimate bending strength of thin-walled steel columns. Sun and Guo [6] measured the high-cycle fatigue damage based on electrical resistance change. Sánchez-Santana [7] studied the effect of fatigue damage on the dynamic tensile behavior of 6061-T6 aluminum alloy and AISI 4140T steel.

In terms of numerical simulation studies, current research mainly focuses on fatigue crack initiation and propagation. Xin et al. [8,9] considered the damage accumulation under cyclic loading based on the SWT damage model and simulated the crack initiation of S355 and S690 through the extended finite element method. Zhang and Ma [10] studied the high-cycle and very-high-cycle fatigue (VHCF) behaviors of AlSi10Mg alloy produced by additive manufacturing and developed a crystal plasticity finite element model (CPFEM) with Voronoi tessellation to simulate the cyclic plastic deformation considering defect effects. Tanaka and Mura [11] first proposed the stress cycle required to calculate the fatigue crack initiation in the slip band based on the crack initiation theory. Based on the Tanaka-Mura crack initiation model, Bruckner [12] first simulated the microcrack initiation process using the finite element method. Jezernik et al. [13] considered that the formation of slip band cracks in the grain was not instantaneous but a slow change process and simulated it in stages.

To sum up, there are few studies on the degradation law and simulation method of mechanical properties of steel after fatigue damage. In this paper, Q355B steel and Q690D steel, which are the most commonly used steel grade for steel structures in China, were examined. Firstly, the changes in mechanical properties of Q355 and Q690 steels with fatigue damage were investigated by static tensile tests. Then, a numerical simulation method for structural steel with fatigue damage was proposed based on the continuous medium damage mechanics model and extended finite element method. Finally, the results obtained from the finite element model were compared with the experimental results to verify the accuracy of the proposed numerical simulation method.

2. Experimental research

In this paper, the experimental scheme is divided into the following three steps: Firstly, five specimens with polished surfaces were tested for high cycle fatigue life under the conditions that loading stress is σ0 and stress ratio is -1. The standard of fatigue failure of specimens was that the loading frequency of the test machine decreased by 5 Hz or cracks appeared on the surface of the specimens. The average value of the fatigue life of the five specimens was taken as the fatigue life Nf of the material under the loading stress of σ0 and the stress ratio of -1. Secondly, according to the linear cumulative damage criterion, high-frequency vibrations were applied to the steel coupons at different times to obtain the pre-fatigue steel specimens with specified damage degrees. Finally, the monotonic tensile loading tests were carried out on pre-fatigue steel coupons to investigate the effects of fatigue damage on the mechanical properties of Q355B and Q690D steel.

2.1. Tensile test on Q355B with pre-fatigue damage

The Q355B specimens were taken from 25 mm thick Q355B steel plates. Cylindric coupons were adopted, and the dimensions were determined according to the Chinese standards GB/T 228.1-2010 and GB/T 3075-2008, as illustrated in Fig. 1.

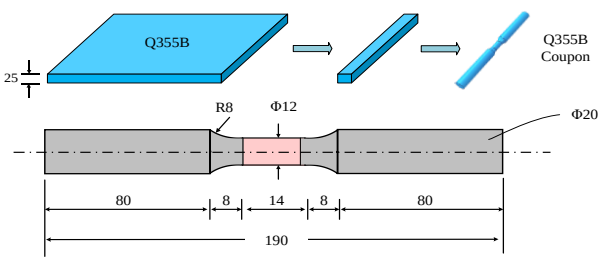

Fig. 1 Dimensional diagram of Q355B specimen (unit:mm)

Fig. 2 QBG-300

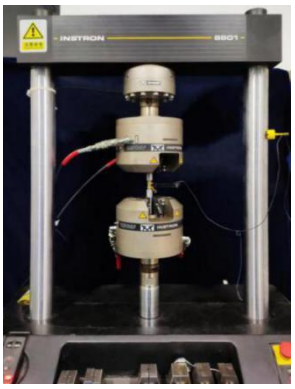

Fig. 3 Instron 8801

The high-cycle fatigue tests were carried out with the QBG-300 high-frequency testing equipment, as shown in Fig. 2. The stress amplitude σ_0 for the Q355B high-cycle fatigue tests was set to 250 MPa with the stress ratio R equal to -1, and the load form was sinusoidal. The fatigue life of five Q355B fatigue specimens was obtained, i.e., 109.5×10^4, 101.8×10^4, 112.1×10^4, 106.2×10^4, and 117.1×10^4. The average life of the five coupons 109.3×10^4 was taken as the high cycle fatigue life N_f of Q355B at this stress amplitude.

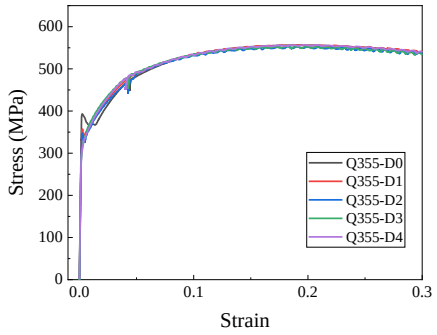

(a) Stress-strain curve

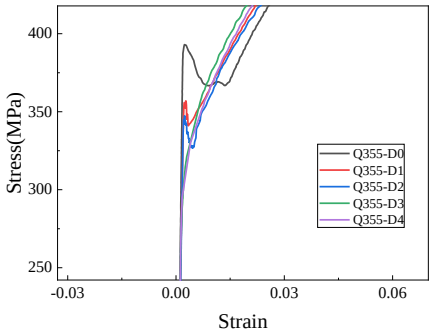

(b) Yield platform

Fig. 4 Mechanical properties of Q355 steel after fatigue damage

Table 1
Mechanical properties of Q355 steel after fatigue damage

Coupons	D	E (MPa)	f_y (MPa)	f_u (MPa)	f_u / f_y
Q355-D0	0.00	215045	388	556	1.44
Q355-D1	0.19	205138	357	556	1.56
Q355-D2	0.37	204337	346	548	1.59
Q355-D3	0.56	199664	330	558	1.69
Q355-D4	0.74	198010	304	557	1.83

With the same stress amplitude and stress ratio, 20×10^4, 40×10^4, 60×10^4, and 80×10^4 cycles of pre-fatigue loading were conducted on the specimens, respectively, and thus the specimens of Q355B steel after fatigue damage were obtained. Miner's linear fatigue accumulation methods were adopted to quantify the fatigue damage degree. Then, monotonic tensile tests were conducted on the pre-fatigued coupons with Instron model 8801, as shown in Fig. 3. The monotonic tensile tests were carried out with displacement control, and the engineering stress-strain curve obtained from the experiment is plotted in Fig. 4, and the main mechanical property parameters are listed in Table 1.

From the test results, with the increase of pre-fatigue damage, the upper yield point and yield plateau on the obtained stress-strain curves disappeared. As the degree of damage increased, the yield strength and elastic modulus tended to decrease [14].

To study the changes of Q355B steel mechanical properties with the degree of damage, the regression analysis was performed, as shown in Fig. 5, where E/E_0, f_y/f_{y0}, f_u/f_{u0} are the ratios of the yield strengths, ultimate strengths, fracture strains, and elastic moduli between the pre-fatigued and undamaged coupons, respectively.

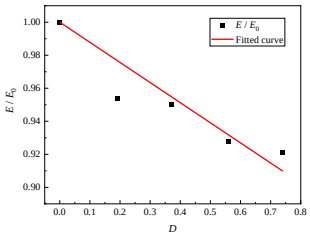

(a) Elastic modulus

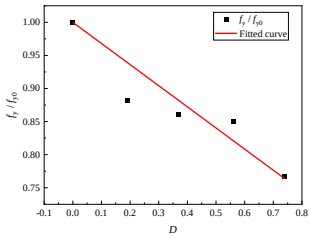

(b) Yield strength

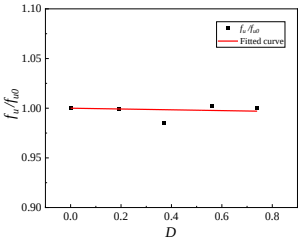

(c) Ultimate strength

Fig. 5 Relationship between mechanical properties and fatigue damage

Comparing the slopes of the regression curves, it shows that the decrease in elastic modulus and yield strength is serious, while the degradation in ultimate strength and fracture strain is little. This indicates that fatigue damage has a significant impact on the elastic mechanical properties of steel. A quantitative relationship between mechanical properties and the degree of damage was established, as expressed in Eq. (1)-(3).

$$E/E_0 = -0.12185D + 1 \qquad R^2 = 0.99981 \qquad (1)$$

$$f_y/f_{y0} = -0.31935D + 1 \qquad R^2 = 0.99851 \qquad (2)$$

$$f_u/f_{u0} = -0.00403D + 1 \qquad R^2 = 0.99994 \qquad (3)$$

2.2. Tensile test on Q690D with pre-fatigue damage

Q690D coupons in the test were taken from 14 mm Q690D steel plates. The experiments were carried out regarding the Q355B test. The geometric dimensions of the Q690D specimens are illustrated in Fig. 6.

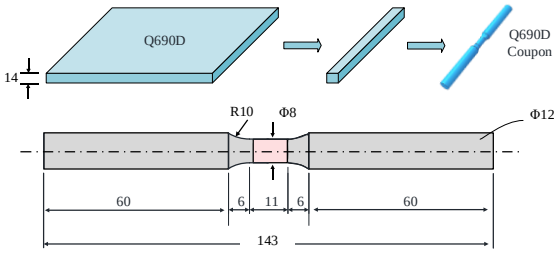

Fig. 6 Geometric dimensions of the Q690D specimens (unit:mm)

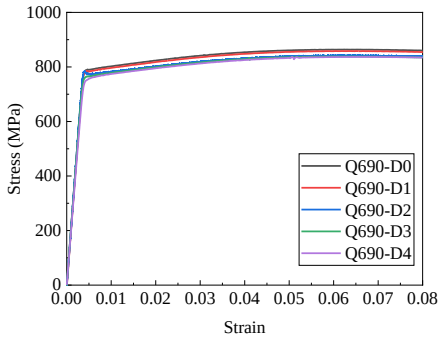

(a) Stress-Strain curve

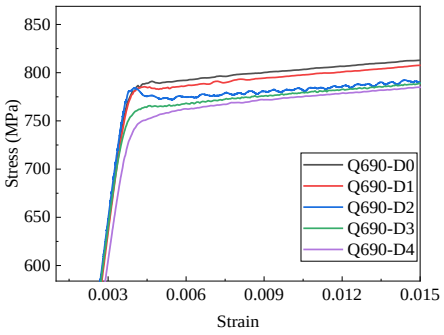

(b) Stress-Strain curve at the yield point

Fig. 7 Mechanical properties of Q690 steel after fatigue damage

The high cycle fatigue tests of Q690D were performed under a stress amplitude of 450MPa and a stress ratio of -1, with the QBG-300 high-frequency testing equipment as well. The fatigue life of the five specimens is 46.7×10^4, 56.8×10^4, 38.9×10^4, 39.5×10^4, and 53.5×10^4 respectively, and the high cycle fatigue life of Q690D at this stress amplitude was set as 50×10^4.

Same as the pre-fatigue loading procedure of Q355B, 20×10^4, 30×10^4, 40×10^4, and 45×10^4 cycles of pre-fatigue loading were conducted on the specimens respectively, to obtain Q690D specimens after fatigue damage. The monotonic tensile tests were conducted on the prepared coupons. During the experiments, the extensometer was taken off when the strain reached 8% before which necking had appeared and the loading force decrease had begun [15]. The engineering stress-strain curves and main mechanical properties can be found in Fig. 7 and Table 2, respectively.

Table 2
Mechanical properties of Q690 steel after fatigue damage

Coupons	D	E (MPa)	f_y (MPa)	f_u (MPa)	f_u / f_y
Q690-D0	0	217100	791	863	1.09
Q690-D1	0.4	216800	784	858	1.09
Q690-D2	0.6	215900	783	853	1.09
Q690-D3	0.8	208500	766	840	1.10
Q690-D4	0.9	202900	761	837	1.10

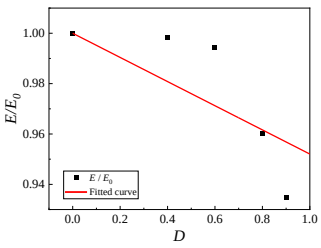

(a) Elastic modulus

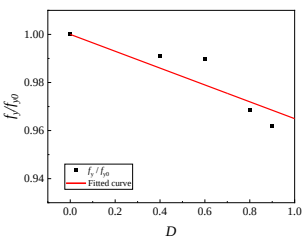

(b) yield strength

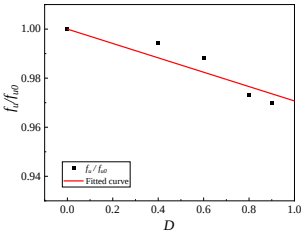

(c) ultimate strength

Fig. 8 Relationship between mechanical properties and fatigue damage

From the experimental result, the influence of fatigue damage on the mechanical properties of Q690D is similar to that of Q355B, and the elastic modulus, yield strength, and ultimate strength of Q690D decrease with the increase of fatigue degree. The variation of the mechanical parameters with the increase of damage variables was described with the normalized parameters, as shown in Fig. 8.

The quantitative relationships between mechanical properties and the pre-fatigue damage degree are established, as expressed in Eq. (4)-(6).

$$E / E_0 = -0.04796D + 1 \qquad R^2 = 0.99965 \tag{4}$$

$$f_y / f_{y0} = -0.03504D + 1 \qquad R^2 = 0.99995 \tag{5}$$

$$f_u / f_{u0} = -0.02929D + 1 \qquad R^2 = 0.99998 \tag{6}$$

3. Numerical simulation methods

3.1. Related theories

The current research on fatigue damage models of metals is mainly divided into the following two categories: The continuous damage mechanics model and the meso-damage mechanics model. Continuous damage mechanics is an image-only approach further developed based on the ductile fracture criterion. It considers the evolution of the microstructure during plastic deformation as an irreversible dissipative process based on the theory of continuous damage mechanics and continuous damage thermodynamics. Kachanov [16] first proposed the concept of continuity in 1958 when studying the problem of the creep of metals. On this basis, Rabotnov [17] proposed the concept of damage degree, as shown in Eq. (7). In the following decades, with the growing interest of scholars, damage mechanics has been continuously developed and has become an increasingly vital tool for the study of material damage.

$$D = 1 - \varphi = 1 - \frac{A}{A_0} \tag{7}$$

where D is the damage degree, A is the effective area, and A_0 is the apparent area of the material. Lemaitre and Chaboche further developed the damage mechanics theory and established the fatigue damage evolution equation based on irreversible thermodynamics and continuous medium mechanics. Li [18] established the fatigue damage evolution equation for the condition of pulsating loads in uniaxial fatigue problems:

$$\frac{\delta D}{\delta N} = \frac{\sigma_m^{(\beta+3)}}{B(\beta+3)(1-D)^{a_2}} \tag{8}$$

where σ_m is the maximum value of the stress cycle when the minimum stress equals 0, B is the material constant, and β and a_2 could be obtained from data fitting with fatigue tests.

According to meso-damage mechanics, the damage of fatigue is the result of the generation and development of micro-defects in materials. These micro-defects include dislocation, slip, micro-voids, and micro-cracks of grains, among which micro-voids and micro-cracks are the main forms of defects. Gurson [19] proposed a method for calculating approximate yield loci via an upper-bound approach for porous ductile materials. Tvergaard and Needleman [20] proposed the Gurson-Tvergaard-Needleman (GTN) model based on the Gurson damage model, considering the interactions between the pores, in which the damage is described as the volume fraction of spherical or ellipsoidal pores.

At the microscale, Angelika Brückner-Foit [21] used the Voronoi method to generate representative volume elements (RVEs) for polycrystalline materials and performed numerical simulations of crack initiation in martensitic steels by introducing the fatigue cracks into the finite element model. M. Mlikota [22] predicted the initiation of short fatigue cracks based on the Tanaka-Mura model and studied the effect of grain size on the fatigue initiation life.

3.2. Simulation method and process

For metallic materials, the whole fatigue damage process mainly consists of the initiation, extended stages of micro-cracks, and the extended stages of long cracks [23, 24]. With most of the fatigue life consumed in the micro-crack stage, the phenomenon on the microscopic scale is the formation and propagation of many micro-cracks in the grain, as shown in Fig. 9. The square hexagon in Fig. 9 represents the grains that make up the material, and the short red lines represent the micro-cracks induced by fatigue loading.

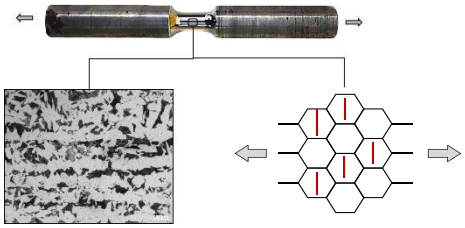

Fig. 9 Schematic diagram of micro-cracks

To define the micro-crack dominated fatigue damage variable, the total number of micro-cracks generated in the specimen under fatigue loading is noted as n, and the length of each micro-crack is noted as CRACK[i]. It is assumed that these micro-cracks are randomly distributed in the specimen. To further simplify the model, the direction of each micro-crack is set to be vertical to the force direction and the projection of each micro-crack in the vertical direction of the force has no overlapping part. With the above assumption, according to the continuous damage mechanics model, the damage degree D of the material specimen is calculated as

$$D = \sum_{i=0}^{n} \mathrm{CRACK}[i] / W \tag{9}$$

where W and L are the width and length of the specimen respectively. In this paper, W and L were taken as the diameter and length of the effective part of the specimen correspondingly. Then the i-th micro-crack would start at (X[i], Y[i]) and end at (X[i], Y[i]+CRACK[i]) as the direction and length of the micro-crack have been determined. Assuming that the micro-cracks are randomly distributed in the vertical direction of the force, the vertical distance (d) between the i+1th micro-crack and the i-th micro-crack is d=random.uniform(0,1)×(1-D)/D×Crack[i+1], as shown in Fig. 10.

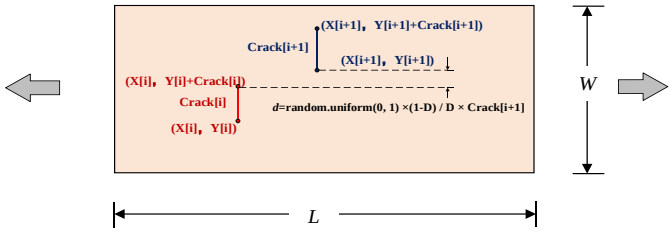

Fig. 10 Coordinates of microcracks

At present, there is no standard criterion for determining fatigue crack emergence, and some scholars [25, 26] take 3-5 times the grain size as the critical value for crack emergence. For structural steel engineering, it is more practical to develop different fatigue crack initiation thresholds depending on the accuracy of the observation, with the crack size at fatigue crack initiation usually being in the range of 0.1 mm to 0.5 mm, while some literature adopts a more precise range (0.25 mm to 0.3 mm). In this paper, it is assumed that the size of the micro-crack is in the range of 0.1mm to 0.3mm.

The simulation of the mechanical properties of steel with pre-fatigue damage could be divided into the following steps:

1. Determine the geometry dimensions W and L of the model, as well as the damage degree (D). Define three integers in Python to represent the above three parameters, and define three empty arrays X[], Y[], and CRACK[], which would be used to store the starting coordinates of each micro-crack in the model and the length of the micro-crack.

2. Define a micro-cracks generating loop with the "while" commend, in which a random line segment of length between 0.1 and 0.3 mm is continuously generated to represent the micro-cracks caused by fatigue damage, and the loop stops until the total length of the generated micro-cracks is greater than D×W, and finally outputs the length of each micro-crack, i.e. CRACK[i].

3. Randomly generate the ordinate of the first micro-crack. Then the ordinate of the starting point of the i+1th micro-crack can be calculated according to the formula in Fig. 11.

4. Random numbers with the same number of micro-cracks were generated in the range of 0.5 to L-0.5 as the abscissa of each micro-crack. To avoid the influence of the too-close distance between two adjacent micro-cracks on the convergence of the FE model, it is assumed that the horizontal distance between two adjacent micro-cracks is greater than 0.3 mm.

The extended finite element method (XFEM) was used to consider the micro-cracks caused by fatigue load. XFEM is suitable for arbitrary boundary conditions, geometric shapes, and nonlinear geometric problems. Based on XFEM, numerical simulations of steel material containing inner micro-cracks were carried out with the general finite element software ABAQUS.

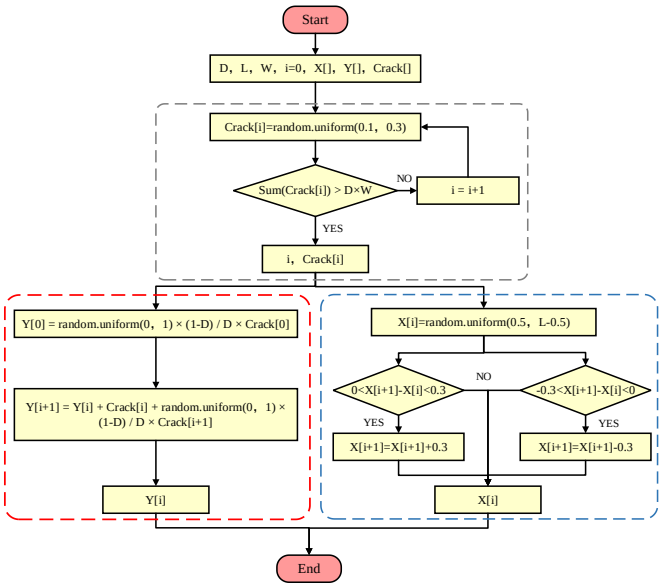

Fig. 11 Flow chart of the modeling

4. Validation of simulation method

To verify the accuracy and reliability of the numerical simulation method proposed in this paper, numerical simulations of pre-fatigued Q355B and Q690D under static tensile loading were carried out using the finite element software ABAQUS. In ABAQUS, the engineering stress-strain curve of the specimen without damage was converted into the true stress-strain curve as the constitutive relationship of the material in the finite element model, and the isotropic hardening was selected as the hardening type of the material. The two-dimensional finite element models corresponding to the geometry of the Q355B and Q690D specimens were established using the CPS4R element.

4.1. Verification and calculation of FE model of Q355B specimen

According to the simulation method of steel after fatigue damage proposed in this paper, the Python programming language was adopted to automatically generate Q355B FE models with different damage degrees corresponding to the pre-fatigue loading test, as shown in Fig. 12.

As mentioned above, the XFEM was used to simulate micro-cracks, as shown in Fig. 13(a). It is worth mentioning that to better reflect the change of yield platform, the lower yield point in the stress-strain curve of Q355b steel obtained from the test was selected as the yield stress when defining the material properties. The boundary conditions of the FE model are as follows: the left boundary was fixed, and the reference point was defined to couple the right side surface to apply displacement load to the specimen, as shown in Fig. 13(b).

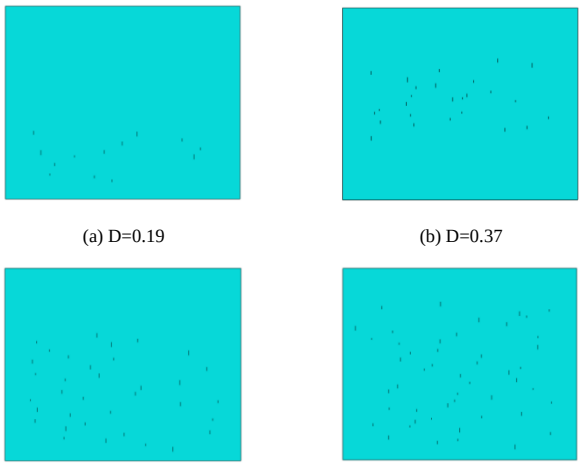

(a) D=0.19 (b) D=0.37

(c) D=0.56 (d) D=0.74

Fig. 12 Finite element model of Q355 after fatigue damage

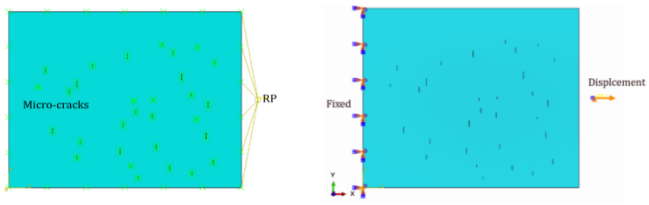

(a) Interaction (b) Boundary condition

Fig. 13 Specific settings of the FE model

Fig. 14 shows the Mises stress of the Q355B specimen under different fatigue damage degrees. It can be seen that when there is no fatigue damage, the stress distribution of the model is relatively uniform, and necking occurs in the middle of the model. With the introduction of micro-cracks, the stress concentration at the crack tip is obvious, and the necking position of the FE model is different from that of the non-damage model.

The STATUSXFEM of the FE model when the step time is 0 is shown in Fig. 14(d). It can be seen that the value of STATUSXFEM at the micro-crack is 1.0 when the analysis step time is 0, that is, when the FE model starts to calculate, which indicates that the displacement on both sides of the micro-crack is discontinuous, and the crack is successfully considered.

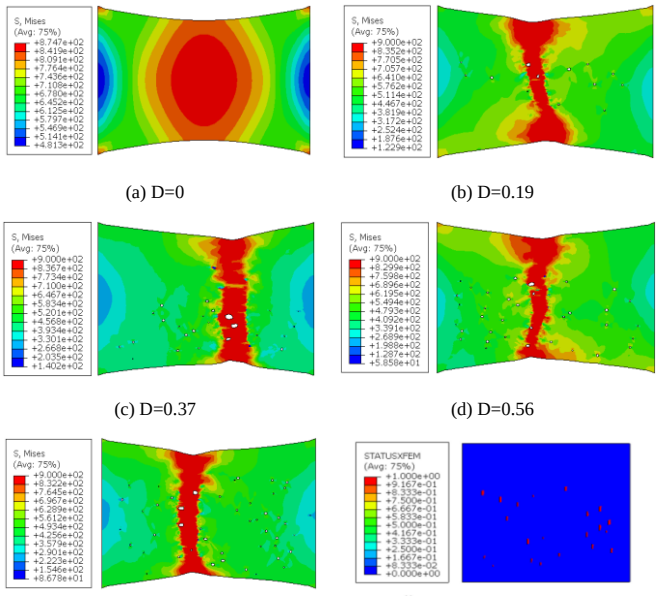

(a) D=0 (b) D=0.19

(c) D=0.37 (d) D=0.56

(d) D=0.74 (d) STATUSXFEM

Fig. 14 Nephogram of the finite element model of Q355

The engineering stress-strain curve of the Q355 specimen under different damage degrees obtained by simulation was shown in Fig. 15. It reflects that the yield platform of Q355 steel gradually disappears with the increase of fatigue degree. The yield strength of Q355B steel decreases with the increase of fatigue strength, and the variation trend of the FE results is consistent with the test results.

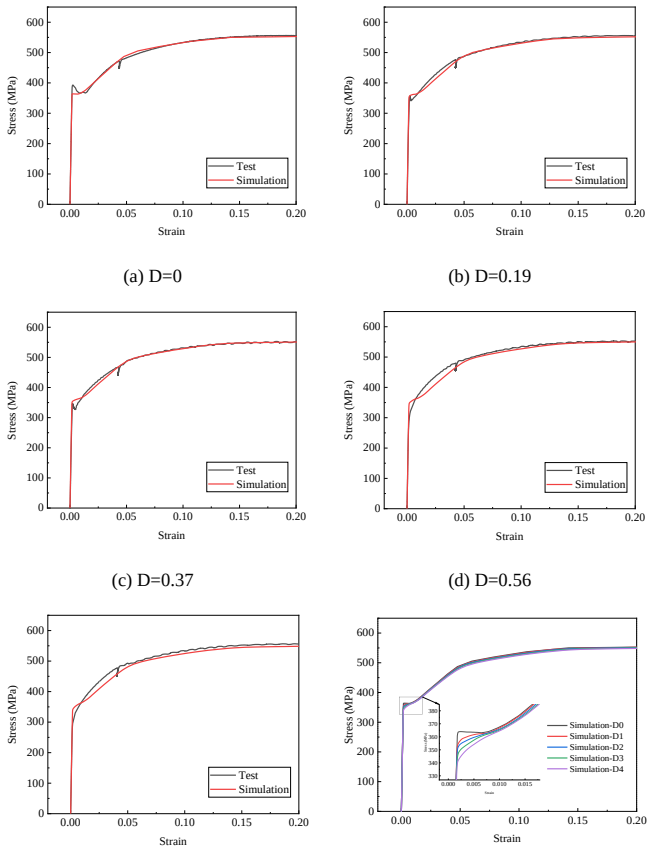

(a) D=0 (b) D=0.19

(c) D=0.37 (d) D=0.56

(e) D=0.74 (f) simulation results

Fig. 15 Comparison of calculation results of Q355B FE models

The yield and ultimate strengths obtained from the simulation were compared with the test values, as shown in Table 3. For the Q355B material after fatigue damage, the maximum difference between the yield strength obtained by the FE simulation and the experimental results is 7.57%, and the maximum difference between the ultimate strength obtained by the FE simulation and the experimental value is 1.80%, which shows the accuracy of the simulation method.

Table 3
Comparison between FE and test results of Q355B

D	f_y (MPa)			f_u / (MPa)		
	FE	Test	Deviation (%)	FE	Test	Deviation (%)
0.19	353	357	1.12	551	556	0.90
0.37	349	346	0.87	550	548	0.36
0.56	339	330	2.73	549	558	1.61
0.74	327	304	7.57	547	557	1.80

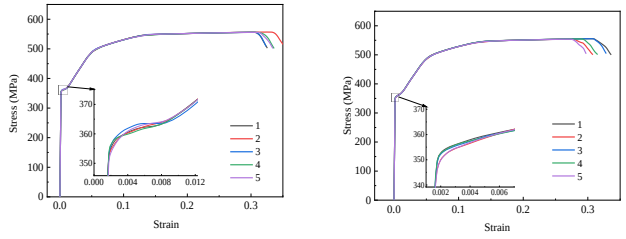

(a) D=0.19 (b) D=0.37

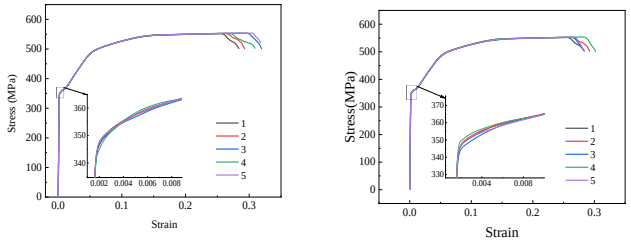

(c) D=0.56 (d) D=0.74

Fig. 16 Results of Q355B FE models

To avoid accidental errors and fully verify the feasibility of the simulation method proposed in this paper, five corresponding finite element models were generated for each damage degree and calculated, and the results obtained are shown in Fig. 16.

The stiffness, yield strength, and ultimate strength calculated by the finite element method have little change in the same damage degree, and the curves obtained by the finite element method almost coincide with the experimental results, which indicates that the simulation method proposed in this paper has good stability and accuracy for Q355B steel.

4.2. Verification and calculation of FE model of Q690D specimen

Based on the simulation method proposed in this paper, the finite element models of Q690 with different damage levels corresponding to the pre-fatigue loading tests were established in ABAQUS. The geometric dimensions of the generated finite element model refer to the dimensions of the effective section. The contact, mesh, and boundary conditions of the Q690 FE model are consistent with those of the Q355B FE model.

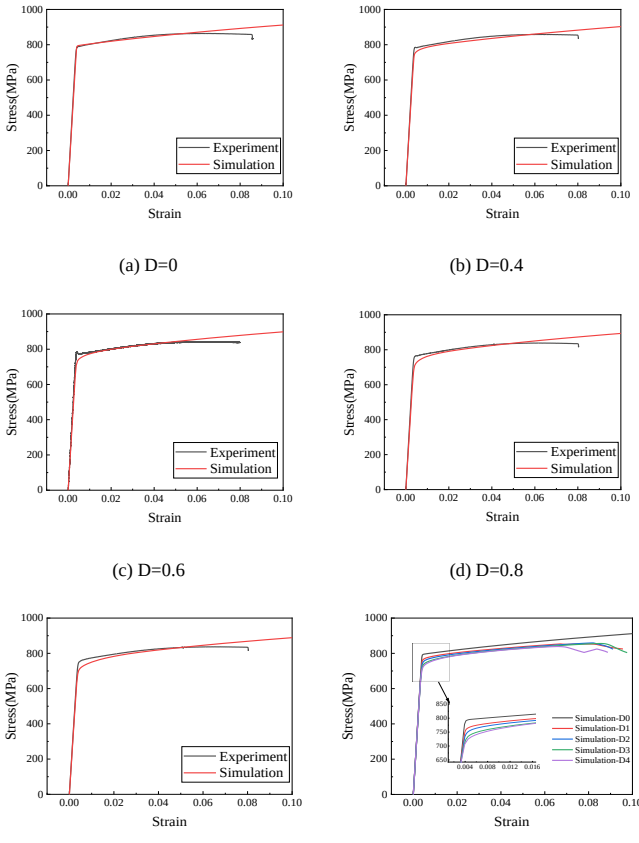

(a) D=0 (b) D=0.4

(c) D=0.6 (d) D=0.8

(e) D=0.9 (f) simulation results

Fig. 17 Comparison of calculation results of Q690D FE models

Fig. 17 shows the comparison between the engineering stress-strain curves of the Q690D specimen under different damage degrees obtained by finite element simulation and the test results. The yield and ultimate strengths obtained from the simulation were compared with the test values, as shown in Table 4.

Table 4
Comparison between FE and test results of Q690D

D	f_y (MPa)			f_u / (MPa)		
	FE	Test	Deviation (%)	FE	Test	Deviation (%)
0.4	757	784	3.44	877	858	2.21
0.6	744	783	4.98	876	853	2.70
0.8	725	766	5.35	872	840	3.81
0.9	711	761	6.57	863	837	3.11

According to the comparison results, for the Q690D material after fatigue damage, the maximum difference between the yield strength obtained by the FE simulation and the experimental value is 6.57%, and the maximum difference between the ultimate strength obtained by the FE simulation and the experimental value is 3.81%. It can be seen that the simulation values are in good agreement with the test values, indicating the feasibility of the simulation method proposed in this paper.

Similar to the numerical simulation of the Q355B specimen, five FE models corresponding to Q690 steel in each damage degree were established and calculated. The calculation results are shown in Fig. 18. The curves under the same damage state are almost coincident and consistent with the experimental values, which shows that the proposed method has good accuracy and stability for Q690D steel.

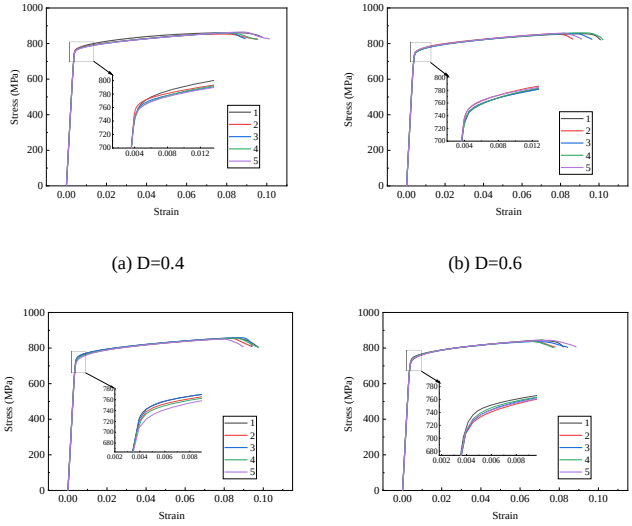

(a) D=0.4 (b) D=0.6

(c) D=0.8 (d) D=0.9

Fig. 18 Results of Q690D FE models

5. Conclusions

The residual mechanical properties of Q355B and Q690D structural steel after exposure to varying degrees of pre-fatigue damage were investigated in the present study. The main conclusions are as follows:

(1) Under monotonic loading, with the increase of pre-fatigue damage, the Young's modulus and yield strength of Q355B steel tended to decrease, and the yield plateau in the stress-strain curve gradually disappeared, while the ultimate strength remained effectively unchanged.

(2) The change of mechanical properties of Q690D after fatigue damage is similar to that of Q355B, but the change of ultimate strength of Q690D after the damage is more obvious than that of Q355B.

(3) The numerical simulation method of steel after fatigue damage proposed in this paper can accurately simulate the mechanical properties of Q355B and Q690D after fatigue damage.

Acknowledgement

The reported research work was sponsored by the National Key Research and Development Program of China (2018YFC1504304).

References

[1] Moćko W, Brodecki A, Radziejewska J. Effects of pre-fatigue on the strain localization during tensile tests of DP 500 steel at low and high strain rates[J]. The Journal of Strain Analysis for Engineering Design, 2015, 50(8): 571-583.

[2] Cockings H L, Cockings B J, Perkins K M. On the effect of pre-strain and pre-fatigue on the monotonic behaviour of ultra-high strength steels[J]. Heliyon, 2020, 6(7): 4440.

[3] Zhang C, Wang R, Song G. Effects of pre-fatigue damage on mechanical properties of Q690 high-strength steel[J]. Construction and Building Materials, 2020, 252: 118845.

[4] Wu Z. Investigation for the relation between the fatigue damage and the degeneration of mechanical properties in metal materials[J]. Journal of Mechanical Strength, 2001, 23(2): 216-218.

[5] Tang Z, Hu X, Jiang J, et al. Effects of pre-fatigue damages on ultimate strength of steel columns: From material to structure[J]. Journal of Constructional Steel Research, 2022, 195: 107358.

[6] Sun B, Guo Y. High-cycle fatigue damage measurement based on electrical resistance change considering variable electrical resistivity and uneven damage[J]. International Journal of Fatigue, 2004, 26(5): 457-462.

[7] Sánchez-Santana U, Rubio-González C, Mesmacque G, et al. Effect of fatigue damage on the dynamic tensile behavior of 6061-T6 aluminum alloy and AISI 4140T steel[J]. International Journal of Fatigue, 2009, 31(11-12): 1928-1937.

[8] Xin H, Veljkovic M. Fatigue crack initiation prediction using phantom nodes-based extended finite element method for S355 and S690 steel grades [J]. Engineering Fracture Mechanics, 2019, 214: 164-176.

[9] Xin H, Correia J A F O, Veljkovic M. Three-dimensional fatigue crack propagation simulation using extended finite element methods for steel grades S355 and S690 considering mean stress effects [J]. Engineering Structures, 2021, 227: 111414.

[10] Zhang W, Hu Y, Ma X, et al. Very-high-cycle fatigue behavior of AlSi10Mg manufactured by selected laser melting: Crystal plasticity modeling[J]. International Journal of Fatigue, 2021, 145: 106109.

[11] Tanaka K, Mura T. A dislocation model for fatigue crack initiation[J]. Journal of applied mechanics, 1981, 48, 97-103.

[12] Brückner-Foit A, Huang X. Numerical simulation of micro-crack initiation of martensitic steel under fatigue loading[J]. International journal of fatigue, 2006, 28(9): 963-971.

[13] Glodež S, Jezernik N, Kramberger J, et al. Numerical modelling of fatigue crack initiation of martensitic steel[J]. Advances in Engineering Software, 2010, 41(5): 823-829.

[14] Si Q, Ding Y, Zong L, et al. Effect of pre-fatigue damage on static and hysteretic behavior of Q355 steel[J]. International Journal of Fatigue, 2022, 160: 106874.

[15] Zong L, Liu H, Si Q, Chung K. Pre-fatigue damage on the mechanical properties of Q690D steel[J]. International Journal of Fatigue, 2022. (under review)

[16] Kachanov L M. Time of the rupture process under creep conditions[J]. Izv AN SSSR Otd Tekhn Nauk, 1958, 8:26-31.

[17] Rabotnov Y N. Paper 68: On the equation of state of creep[C]. Proceedings of the Institution of Mechanical Engineers, Conference Proceedings. Sage UK: London, England: SAGE Publications, 1963, 178(1): 2-117-2-122.

[18] Sun B, Li Z. A multi-scale damage model for fatigue accumulation due to short cracks nucleation and growth[J]. Engineering Fracture Mechanics, 2014, 127: 280-295.

[19] Gurson A L. Continuum theory of ductile rupture by void nucleation and growth: Part I—Yield criteria and flow rules for porous ductile media[J]. 1977.

[20] Tvergaard V, Needleman A. Analysis of the cup-cone fracture in a round tensile bar[J]. Acta metallurgica, 1984, 32(1): 157-169.

[21] Brückner-Foit A, Huang X. Numerical simulation of micro-crack initiation of martensitic steel under fatigue loading[J]. International journal of fatigue, 2006, 28(9): 963-971.

[22] Mlikota M, Dogahe K, Schmauder S, et al. Influence of the grain size on the fatigue initiation life curve[J]. International Journal of Fatigue, 2022, 158: 106562.

[23] Hussain K, De Los Rios E R, Navarro A. A two-stage micromechanics model for short fatigue cracks[J]. Engineering Fracture Mechanics, 1993, 44(3): 425-436.

[24] Hong Y, Qiao Y. An analysis on overall crack-number-density of short-fatigue-cracks[J]. Mechanics of materials, 1999, 31(8): 525-534.

[25] Ge L. Predicting Fatigue Life Based on the Behavior of Short Fatigue Crack[J]. Materials For Mechanical Engineering, 2001. 25(2), 18-20. (in chinese)

[26] Wu Z. Statistical Investigation for the Behavior of Short Fatigue Cracks in Medium Carbon Steel[J]. Journal of Mechanical Strength, 20(4), 295-299 ,1998. (in chinese)